Journal of Power Sources 185 (2008) 1218–1224

Contents lists available at ScienceDirect

Journal of Power Sources

journal homepage: www.elsevier.com/locate/jpowsour

Neodymium-deficient nickelate oxide $Nd_{1.95}NiO_{4+\delta}$ as cathode material for anode-supported intermediate temperature solid oxide fuel cells

C. Lalanne[a,*], G. Prosperi[b,1], J.-M. Bassat[a], F. Mauvy[a], S. Fourcade[a], P. Stevens[c], M. Zahid[d], S. Diethelm[b], J. Van herle[b], J.-C. Grenier[a]

[a] CNRS, Université de Bordeaux, ICMCB, 87 avenue du Dr. A. Schweitzer, Pessac, F-33608, France
[b] Laboratory of Industrial Energy Systems (LENI), ME A2 Station 9, Faculty of Engineering (STI), Ecole Polytechnique Fédérale de Lausanne (EPFL), CH-1015 Lausanne, Switzerland
[c] EDF R&D, Av. des Renardières, F-77818, Morte sur Loing-Cedex, France
[d] EDF-EifER Emmy-Noether-Strasse 11, 76131 Karlsruhe, Germany

ARTICLE INFO

Article history:
Received 13 March 2008
Received in revised form 23 June 2008
Accepted 28 June 2008
Available online 6 July 2008

Keywords:
Solid oxide fuel cells
Cathode
Nickelate oxide
Impedance spectroscopy

ABSTRACT

The neodymium-deficient nickelate $Nd_{1.95}NiO_{4+\delta}$, mixed conducting K_2NiF_4-type oxide, was evaluated as cathode for solid oxide fuel cells. The electrochemical properties were investigated on planar Ni–YSZ anode-supported SOFC based on co-tape casted and co-fired HTceramix® cells. Using a layer of strontium doped lanthanum cobaltite as current collector, a current density of 1.31 A cm^{-2} (at 0.70 V) was obtained at 800 °C using hydrogen fuel with small single cells, after optimizing the cathode sintering temperature. Impedance spectroscopy measurements were performed; the different resistive contributions and the values of the corresponding equivalent capacities are discussed.

1. Introduction

Among the major efforts devoted to SOFC development, one of the long-established drawbacks is the cathode material optimization. A current challenge is to obtain electrodes having high activity for electrochemical oxygen reduction in the 600–700 °C operating temperature range as well as low area specific resistances.

Most published results have focused the traditional oxygen-deficient $AMO_{3-\delta}$ perovskite-type compounds [1–4].

Since 1999, a few research groups have oriented their studies towards oxygen over-stoichiometric materials [5–9]. Several members of the Ruddlesden–Popper oxide family ($A_{n+1}M_nO_{3n+1}$) have been characterized as potential cathode materials ($n = 1$, 2 and 3) [9–10]). The mixed ionic and electronic conduction (MIEC) as well as interesting catalytic properties for oxygen reduction make them promising cathode candidates.

At the ICMCB laboratory, the most important investigations were dedicated to the $n = 1$ member of this oxide family, $Ln_{2-x}A_xMO_{4\pm\delta}$, with Ln as lanthanide, A as alkaline-earth cation or vacancy, and M as transition metal. Among the prepared compounds (Ln = La, Pr, Nd; A = Sr, Ca and M = Cu, Ni, Co) [5,11], the $Nd_{1.95}NiO_{4+\delta}$ composition was selected for this study because it shows both a large over-stoichiometry δ in the whole temperature range 0–900 °C, (for example, $\delta = 0.17$ at 700 °C), and Nd deficiency, which is expected to decrease the chemical activity of the material against solid-state reaction with the electrolyte. In addition, the 2D-type $A_2MO_{4+\delta}$ structure shows peculiar transport properties in comparison with the isotropic perovskite structure. Thus, Bassat et al. [12] evidenced the anisotropy of the anionic conductivity in $La_2NiO_{4+\delta}$ single crystals.

Furthermore, the thermal expansion coefficient (TEC) was calculated from both high temperature X-ray diffraction analyses and dilatometry measurements; they show a rather good mechanical compatibility with usual electrolytes ($12.7 \times 10^6\ K^{-1}$, $13 \times 10^6\ K^{-1}$ and $13.6 \times 10^6\ K^{-1}$ respectively for $Nd_2NiO_{4+\delta}$, $La_2NiO_{4+\delta}$ and $Pr_2NiO_{4+\delta}$ oxides) [6].

In previous work, porous layers of the cathode material (nickelate powder prepared by a polyacrylamide gel route) were coated on dense 8YSZ pellets using a brush in order to evaluate the electrochemical performances of the Nd stoichiometric compound $Nd_2NiO_{4+\delta}$ [13]. For instance, the electrochemical behaviour of symmetrical cells $Nd_2NiO_{4+\delta}$/YSZ/$Nd_2NiO_{4+\delta}$, under

* Corresponding author. Tel.: +33 5 40 00 25 91; fax: +33 5 40 00 27 61.
E-mail address: lalanne@icmcb-bordeaux.cnrs.fr (C. Lalanne).
[1] resent address: SOFCpower, via Al Dos de la Roda, 60, 38057 Pergine Valsugana, Italy.

0378-7753/$ – see front matter © 2008 Elsevier B.V. All rights reserved.
doi:10.1016/j.jpowsour.2008.06.072

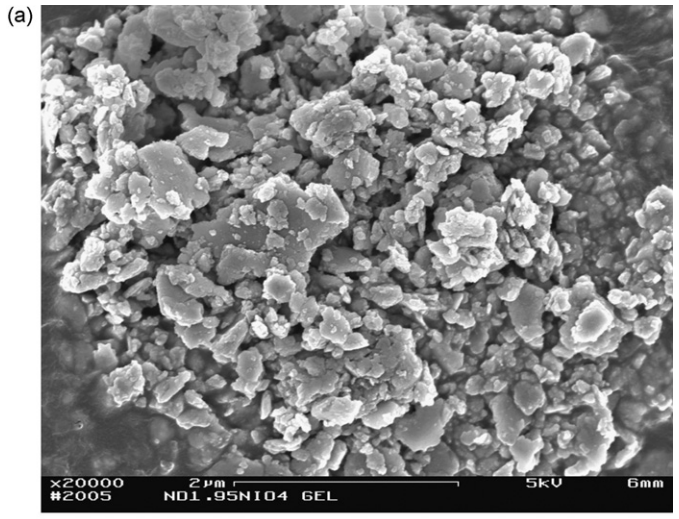

Fig. 1. SEM micrograph and particle size distribution of $Nd_{1.95}NiO_{4+\delta}$ powder after the attrition stage.

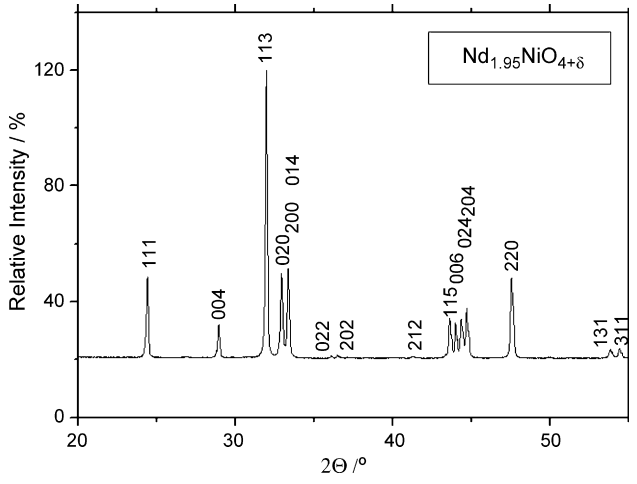

Fig. 2. X-ray diffraction pattern for $Nd_{1.95}NiO_{4+\delta}$ oxide.

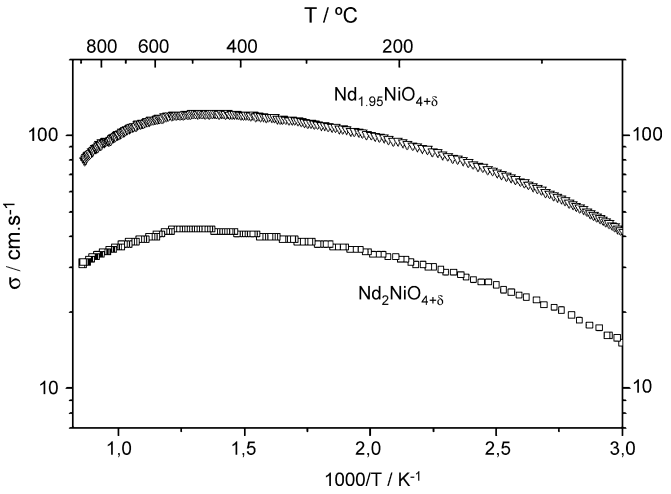

Fig. 3. Thermal variation of the electrical conductivity measured by the four probe method for $Nd_{1.95}NiO_{4+\delta}$ oxide.

Table 1
Oxygen diffusion D^* and surface exchange k coefficients measured at 700 °C

Cathode material	$Nd_{1.95}NiO_{4+\delta}$	$Nd_2NiO_{4+\delta}$
D^* ($cm^2\ s^{-1}$)	5×10^{-8}	4.6×10^{-8}
k ($cm\ s^{-1}$)	1.5×10^{-6}	3×10^{-7}

air (impedance spectroscopy and voltammetry measurements) revealed a cathodic area specific resistance (ASR) of about 0.5 Ω cm^2 at 700 °C. First experiments on a 5-cell stack (250 cm^2) led to a power density of 0.32 W cm^{-2} at 750 °C with an electrical efficiency of 35%. However, delamination of the cathodes was observed after operating for 800 h [14].

In this work, we aim to study the optimization of the cathode fabrication in order to avoid such delamination and to lower the cathode/YSZ interfacial resistance which has been shown to be the most penalizing for decreasing the cell ASR value [15].

2. Experimental

2.1. Preparation and characterizations of $Nd_{1.95}NiO_{4+\delta}$ oxide

The oxide was prepared by the polyacrylamide gel route [16]. Aqueous solutions of each cation were made from nitrate salts and

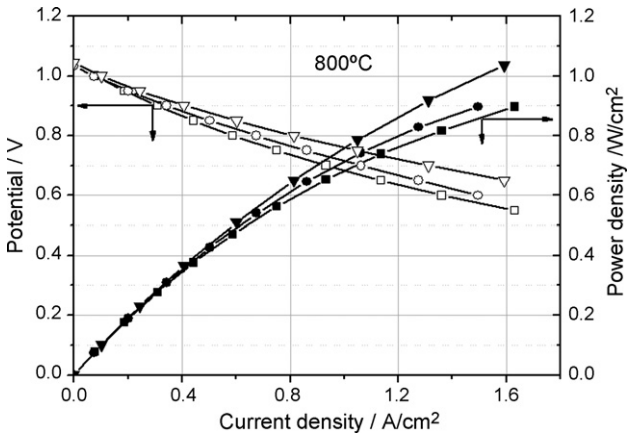

Fig. 4. *i–V–P* curves measured after 24 h polarization (0.50 A cm^{-2}; 800 °C) for $Nd_{1.95}NiO_{4+\delta}$ cathode sintered at various temperatures: □, ■ 1000 °C (A-type); ○, ● 1050 °C (B-type) and ▽, ▼ 1100 °C (C-type).

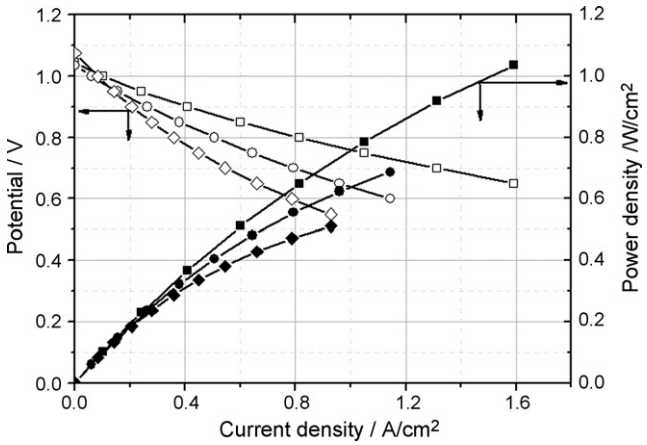

Fig. 5. *i–V–P* curves measured at 700 °C (◊, ♦), 750 °C (○, ●) and 800 °C (□, ■) on the C-type cell ($Nd_{1.95}NiO_{4+\delta}$ sintered at 1100 °C).

the cations were then chelated by triammonium citrate (pH controlled via NH_4OH). Solutions of the chelated cations were mixed in a stoichiometric ratio. The organic gel was made using monomers of acrylamide and *N*,*N*′-methylene-bis-acrylamide as cross-linker. The polymerization initiator α,α′-azoisobutyronitrile (AIBN) dissolved in a few ml of acetone was used. This gel was heated in a porcelain bowl at 800 °C for 1 h in a ventilated furnace. Final annealing at 1000 °C for 12 h was necessary to obtain a single phase.

The as-prepared powder was finally attrited: the particle size distribution measured with a Malvern® laser granulometer is given in Fig. 1. The average particle size $D_{0.5}$ is around 0.4 μm (volume statistics). The powder was examined by scanning electron microscopy (JEOL JSM 6360 A) after the attrition stage (Fig. 1).

This oxide was characterized by X-ray diffraction using a Philips PW1050 diffractometer (Cu Kα radiation). The sample revealed a single-phase material exhibiting the K_2NiF_4-type structure with orthorhombic symmetry (*Bmab* space group) (Fig. 2). The total electrical conductivity was measured using the four probe method on dense pellets sintered at 1350 °C; the result is reported in

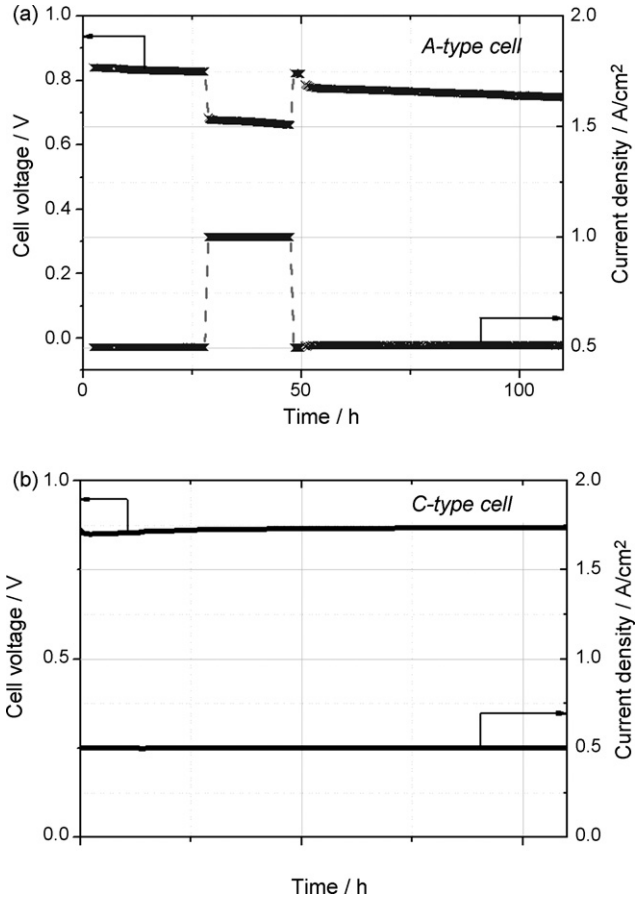

Fig. 6. Time dependence of the polarization at 800 °C for (a) A- and (b) C-type cells.

Fig. 3. For comparison, the electrical conductivity of the stoichiometric compound $Nd_2NiO_{4+\delta}$ is also shown. The Nd-deficient oxide $Nd_{1,95}NiO_{4+\delta}$ exhibits a higher electronic conductivity. Furthermore, oxygen diffusion coefficient D^* and surface exchange

Table 2
Different thermal treatments of the cathodic layer

Cathode type	A	B	C	D
Sintering temperature, °C (dwell time, h)	1000(4)	1050(4)	1100(4)	1200(4)

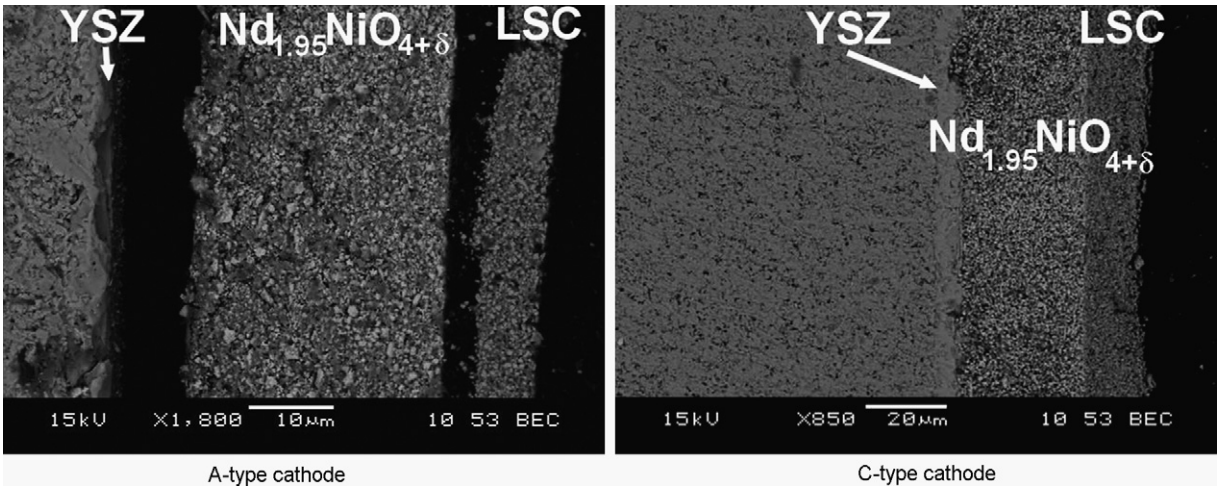

Fig. 7. SEM micrographs of the cells after polarization (100 h; 0.50 A cm^{-2}).

Table 3
Current densities measured after a 24-h polarization stage at 0.50 A cm^{-2}, at 800 °C

Cathode type	A	B	C	D
Sintering temperature (°C)	1000	1050	1100	1200
Current density (A cm^{-2}) @ 0.70 V and 800 °C	0.93	1.06	1.31	n. a.
Total ASR (Ω cm^2)	0.260	0.241	0.183	n. a.

coefficient k have been measured using the $^{18}O/^{16}O$ isotope exchange depth profile technique (IEDP) and the analyses by secondary ion mass spectroscopy (SIMS) on dense membranes [6]. The results obtained at 700 °C are given in Table 1. It can be observed that the surface exchange coefficient k is higher for the Nd-site deficient oxide, which confers interesting catalytic properties. In addition, in previous works, the results had been compared to perovskites and showed an important improvement, between 1 and 7 orders of magnitude for D^* coefficients compared to those of LSFC ($La_{0.6}Sr_{0.4}Fe_{0.8}Co_{0.2}O_{3-\delta}$), LSFN ($La_{0.6}Sr_{0.4}Fe_{0.8}Ni_{0.2}O_{3-\delta}$) and LSM ($La_{0.8}Sr_{0.2}MnO_{3-\delta}$) oxides, and between 1 and 2 orders of magnitude for the corresponding k coefficients [17,18].

2.2. Cell fabrication

Thin anode-supported half cells (ASE) were provided by HTceramix S.A. (40 mm × 40 mm) (http://www.htceramix.ch): they are made of planar Ni–zirconia cermets (with a thickness in the range 180–280 μm) supporting a 6–8 μm 8YSZ electrolyte, both prepared by tape-casting and co-fired [19,20]. Cathodes were deposited by screen-printing of a terpineol-based slurry. The effective cathode surface area was 10 mm × 10 mm. The final sintering program was as follows: an initial ramp at 1 °C min^{-1} up to 400 °C to eliminate organic compounds, followed by a temperature increase up to the sintering temperature at 5 °C min^{-1}. Various sintering temperatures were selected (1000, 1050, 1100 and 1200 °C for 4 h) in order to study the influence on the performances of the single cells.

In addition, a current collector layer, the perovskite-type cobaltite $La_{1-x}Sr_xCoO_{3-\delta}$ of high electrical conductivity ($\sigma > 10^3$ S cm^{-1} at 700 °C [21]) was screen-printed on the nickelate layer, without being sintered. In addition, it was checked no significant reactivity with the nickelate to occur provided $T < 800$ °C, even over a long time.

Four types of samples were prepared and respectively labeled A, B, C and D, according to the final temperature sintering (Table 2). The final cathode thickness was about 30 μm.

2.3. Cell characterizations

2.3.1. Electrochemical measurements

The single cell electrical characterizations were performed in a non-sealed set-up configuration. The cells were mounted and pressed between Inconel flanges with porous alumina felts on each side as electrical insulators and gas diffusers. The current collectors were platinum mesh for the cathode side and nickel mesh for the anode. The measurements were conducted in a Rohde®-type furnace. Gas inputs were controlled by rotameters: because of a non-tight system, gas flow rates were typically 250 mL min^{-1} for air and 120 mL min^{-1} for hydrogen. After heating under air, hydrogen was introduced at 800 °C to reduce the cermet for 4 h. An Amel® potentiostat–galvanostat was used to measure polarization and power curves and to perform long-term tests under constant polarization (0.50 A cm^{-2}). The open circuit voltage (OCV) was checked for each cell (1.00 < OCV < 1.10 V at 800 °C) before polarization. The different cells were systematically characterized by electrochemical impedance spectroscopy (EIS) at OCV with a 50 mV modulation amplitude (Autolab® PGSTAT 30) in the frequency range 10^5 Hz to 5 mHz.

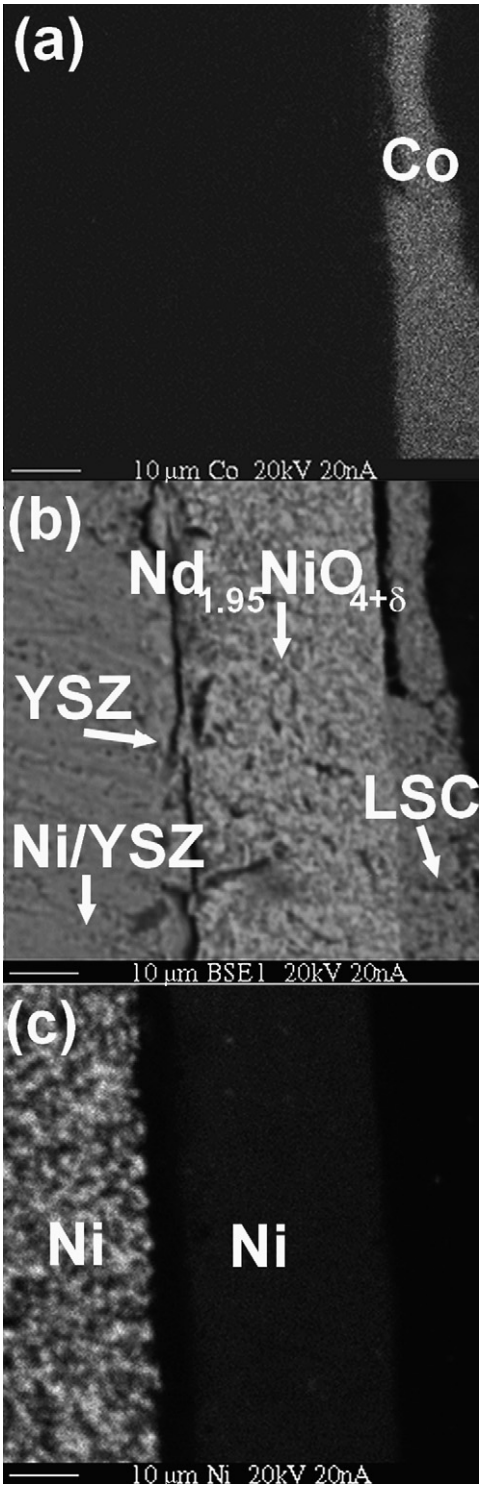

Fig. 8. Analysis of the A cell after degradation. BSE image (b) and EDX maps of Co (a) and Ni (c).

2.3.2. SEM and EDX characterizations

Scanning electronic microscopy (SEM) analyses were performed with JEOL JSM 6360 A equipment in order to check the different layer microstructures and the adhesion between electrolyte

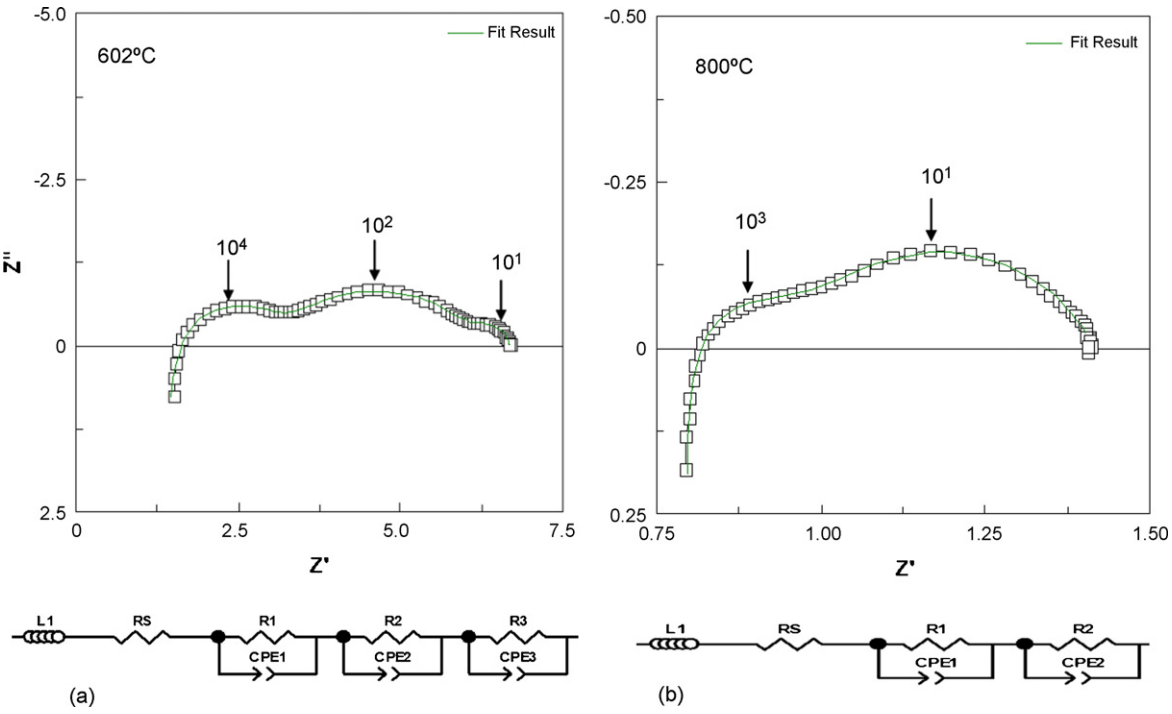

Fig. 9. Experimental impedance spectra (symbol □) and fit (solid line) with the corresponding equivalent circuits depending on operating temperature (602 °C on the left and 800 °C on the right).

and electrodes after polarization. In addition, energy dispersive X-ray (EDX) spectrometry was used to detect potential cation diffusion.

3. Results and performances

The single cells were first characterized at 800 °C in order to select the best performing one. Then, detailed electrochemical characterizations were performed on the selected cell, at different operating temperatures, 800, 750 and 700 °C, with the aim of studying the behaviour of this cathode material at temperatures as low as 700 °C.

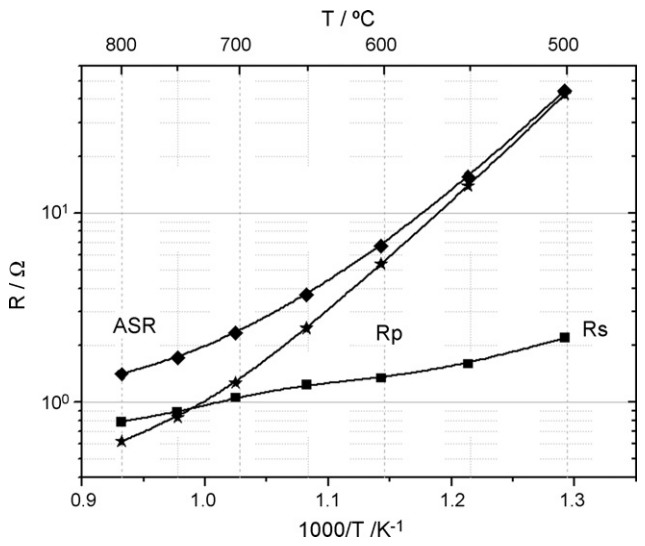

Fig. 10. Ohmic resistance R_s, polarization resistance R_p and total ASR measured on $Nd_{1.95}NiO_{4+\delta}$/8YSZ/Ni–8YSZ (C-type cell, cathode sintered at 1100 °C).

3.1. Influence of the sintering thermal cycle

After the sintering processes, the D cell sintered at 1200 °C showed large cracks on the whole cathode surface. This sample was not kept for further electrochemical characterizations.

For A, B and C single cells, the measured OCV was in the range 1.03–1.06 V at 800 °C. Polarization (*i*–*V*) and power density (*i*–*P*) curves at 800 °C (Fig. 4) were recorded after an initial load at 0.50 A cm^{-2} (the current density usually adopted for medium term tests), for 24 h. This preliminary polarization stage was carried out in order to reach a steady state of the cells in operating conditions [22]. Detailed data of the characteristics at 0.70 V (current density and measured ASR at 0.70 V) are given in Table 3. The best performance, 1.31 A cm^{-2} at 0.70 V, was obtained for sample C with the cathode sintered at 1100 °C.

3.2. Behaviour at different operating temperatures

Additional characterizations were performed on the cell for which the best performances were observed (C-type cathode): *i*–*V*–*P* curves were measured at different operating temperatures, 700, 750 and 800 °C. The results obtained with identical gas flow rates (250 mL min^{-1} for air and 120 mL min^{-1} for hydrogen) are shown in Fig. 5.

At 0.70 V, the current density decreased from 1.31 A cm^{-2} at 800 °C down to 0.79 A cm^{-2} at 750 °C, and 0.54 A cm^{-2} at 700 °C.

These performances can be compared to previous data obtained using the same test set-up: identical studies had been performed with successive layers of manganite LSM and cobaltite LSC as cathode and current collector layers respectively on HTceramix S.A. anode supports [23]. The measured current density at 0.70 V was 0.50 A cm^{-2}, at 750 °C, while the value obtained with the nickelate compound led to a large improvement of about 50%, at this operating temperature. This result was also compared to data extracted from literature. Laberty et al. [24] recently reported a power den-

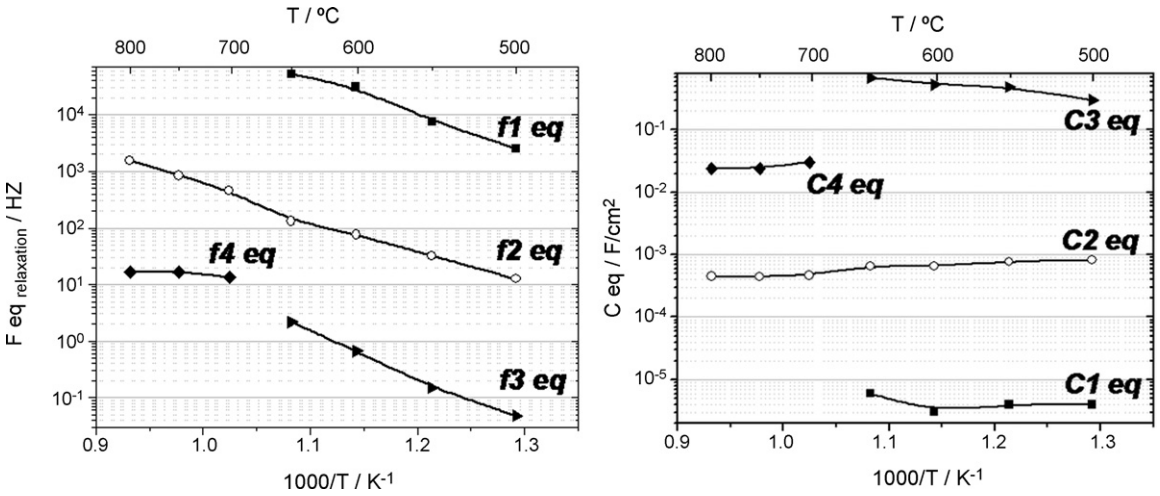

Fig. 11. Arrhenius diagrams of the relaxation frequencies and equivalent capacitances.

sity of 0.25 W cm^{-2} (at 0.70 V), at 800 °C, on dime cells made of the nickelate compound $La_2NiO_{4+\delta}$ painted onto YSZ electrolyte supported on Ni–YSZ anode whereas the ASR value was 0.40 Ω cm^2 at the same temperature. However, comparing electrochemical performances is risky due to considerable differences concerning test cell geometry, current collectors, gas flows, shaping parameters, etc.

For SOFC devices to be viable, high power densities need to be achieved at high electrical efficiency, *i.e.* at sufficiently high cell voltage (>0.70 V) and fuel utilization (>70%). For the 40 mm × 40 mm single cells used in the current study, fuel conversion is very low. Operation with more realistic fuel utilization was previously carried out in a 5 cell-stack (250 cm^2 active surface area, $Nd_2NiO_{4+\delta}$ cathode) obtaining 0.31 W cm^{-2} at 700 °C (≈0.70 V average repeat element voltage) and electrical efficiency of 33% (5 mL min^{-1} cm^{-2} hydrogen flow) [25].

3.3. Short-term polarization

A- and C-type single cells were then polarized for 100 h at 0.50 A cm^{-2}. The potentials measured *vs.* time are shown in Fig. 6a and b. In Fig. 6a, the A-type cell was also polarized at 1.00 A cm^{-2} for 20 h.

The cell behaviour was significantly different: the C-type cell showed a voltage increase from 0.85 to 0.87 V, whereas the A-type cell exhibited a degradation from the beginning, which is amplified with the 1.00 A cm^{-2} polarization, the voltage decreasing from 0.84 to 0.75 V after 100 h.

After polarization, the samples were characterized by SEM. Fig. 7 reports micrographs of both cells; they are arranged so that the anodes are on the left part of the image (cermet/YSZ/$Nd_{1.95}NiO_{4+\delta}$/LSC from left to right).

For the A-type sample, it was observed a significant delamination between the electrolyte and the cathode layer inducing also the delamination of the LSC current collector layer from the nickelate. EDX analyses (Cameca SX 100) were conducted on this cell; nickel and cobalt were probed (Fig. 8). The back scattered electron (BSE) imaging represents the analysed area of the cell (Fig. 8b). The two other micrographs (Fig. 8a and c) show the cobalt and nickel atomic distributions (white dots). It can be concluded from these analyses that no cation migration occurred from electrode or current collector layer towards the electrolyte during polarization, especially no cobalt diffusion. The potential drop observed when the nickelate was sintered at 1000 °C, seems to result from the poor mechanical adhesion between the different layers. A sintering temperature of 1100 °C seems to be required to obtain a good adhesion of the cathode on the electrolyte.

3.4. Electrochemical impedance spectroscopy characterization

Electrochemical characterizations were performed on a C-type cell (cathode sintered at 1100 °C). The LSC current collector layer was replaced by a $Nd_{1.95}NiO_{4+\delta}$ layer with the aim to simplify the interpretation of the results (no additional contribution). Typical EIS diagrams are reported in Fig. 9. The ohmic cell resistance R_s (high frequency intercept), the polarization resistance R_p (between low and high frequency intercepts) and the total area specific resistance ($R_s + R_p$) measured in the temperature range 500–800 °C are given Fig. 10. As expected, R_s is a little larger than when using a LSC layer, which can be correlated to a poorer electronic current collection. The R_p represents the major part of the total ASR up to 750 °C, whereas R_s becomes predominant at 800 °C. This result gives some information about the limiting contribution as a function of the operating temperature: the electrolyte/electrode interface and the electrode reactions (taken into account in R_p) are penalizing in the 500–750 °C range whereas the electrolyte and the electrode ohmic resistances as well as the various current collector contributions, all included in R_s, represent the most resistive contribution starting above 750 °C.

Analysis of the impedance data was carried out in the whole operating temperature range. The spectra (Fig. 9) were generally composed of two or three semi-circles depending on operating temperature. The data could be fitted using the following equivalent circuits: $L+R_s+(R_1//CPE_1)+(R_2//CPE_2)+(R_3//CPE_3)$ in the 500–650 °C range (Fig. 9a) and $L+R_s+(R_1//CPE_1)+(R_2//CPE_2)$ from 650 up to 800 °C (Fig. 9b) with L, an inductance, R, a resistance and CPE, a constant phase element $Z_{CPE} = 1/Y_0(j\omega)^n$ [26]. In order to study the electrochemical behaviour of the cell, following the Schouler-type methodology [26], the Arrhenius plots of the different relaxation frequencies and of the equivalent capacitances, given by: $C_{eq} = R^{(1-n)/n} \times CPE^{1/n}$, relating to the various contributions are reported in Fig. 11. The fact that the equivalent capacities are independent of temperature, leads to confirmation of the presence of four different phenomena. In the range 500–650 °C, they are labeled 1, 2 and 3 and beyond 650 °C, the two remaining ones are labeled 2 and 4. Contribution #2 exists in the whole temperature range.

The calculated equivalent capacitances are: $C_{1eq} \approx 10^{-6}$, $C_{2eq} \approx 4\text{–}8 \times 10^{-4}$, $C_{3eq} \approx 5 \times 10^{-1}$ and $C_{4eq} \approx 2 \times 10^{-2}$ F cm^{-2}. The

assignment of chemical and/or electrochemical processes is not straightforward. Available data from the literature deals with symmetrical cells (electrode/electrolyte/electrode) characterized under oxidizing or reducing atmospheres depending on the studied compound, or basic studies performed on dense electrodes [28–30]. The value C_{1eq} (10^{-6} F cm^{-2}) is generally assigned to the ionic transfer at the electrode–electrolyte interface whereas larger capacitances (in the range 10^{-3}–10^{-1} F cm^{-2}) are attributed to electrode processes (oxygen adsorption, diffusion, etc.). Additional impedance measurements have to be performed under specific experimental conditions: (i) under various air and hydrogen flow rates; (ii) under low oxygen partial pressure on the cathode side; (iii) under different fuels (H_2/H_2O/CH_4, etc.) on the anodic side; (iv) under different polarizations. These experiments will help to identify the cathodic and anodic contributions and to determine the different electrochemical processes such as mass transfer, adsorption–desorption, diffusion, etc. [22].

4. Conclusions

A selected $Nd_{1.95}NiO_{4+\delta}$ composition, which is neodymium-deficient and over-stoichiometric in oxygen, was screen-printed as cathode material on anode-supported SOFC half-cell based on co-tape casted 8YSZ/Ni–8YSZ HTceramix® commercial cells. Current density up to 1.31 A cm^{-2} @ 0.70 V and 800 °C has been obtained for cathodes sintered at 1100 °C. In addition, values higher than 0.50 A cm^{-2} at the same voltage were measured at operating temperatures down to 700 °C, showing the potential use of these compounds at intermediate temperatures. Whereas the $A_2MO_{4+\delta}$ compounds are known for their high ionic conductivity and good electrocatalytic properties, their limited electronic conductivity required the use of a current collector such as LSC perovskite, for these experiments.

A first analysis of impedance spectra measured on complete cells without LSC current collector showed that the polarization resistance was larger than the ohmic resistance on almost the whole temperature range. It can be concluded that the electrolyte–electrode interfaces and the electrode reactions (anode and cathode) are the penalizing contributions. The deconvolution of the polarization resistance revealed four contributions depending on the operating temperature: two of them were observed in the range 500–650 °C, one between 700 and 800 °C and the last one in the whole range 500–800 °C. However, additional impedance measurements have to be performed in given experimental conditions (varied gas composition, under polarization, or using reference electrodes) with the aim of assigning definitively the various chemical and/or electrochemical processes to the electrochemical responses.

Acknowledgment

The authors are indebted to HTceramix S.A. for supply of the SOFC components.

References

[1] Z. Shao, S. Haile, Nature 431 (2004) 170–173.
[2] P. Hjalmarsson, M. Sogaard, A. Hagen, M. Mogensen, Solid State Ionics 179 (17–18) (2008) 636–646.
[3] F. Tietz, V.A.C. Haanappel, A. Mai, J. Mertens, D. Stöver, J. Power Sources 156 (1) (2006) 20–22.
[4] T. Hibino, A. Hashimoto, T. Inoue, J. Tokuno, S. Yoshida, M. Sano, Science 288 (2000) 2031–2033.
[5] E. Boehm, J.M. Bassat, M.C. Steil, P. Dordor, F. Mauvy, J.C. Grenier, Solid State Sci. 5 (7) (2003) 973–981.
[6] E. Boehm, J.M. Bassat, P. Dordor, F. Mauvy, J.C. Grenier, P. Stevens, Solid State Ionics 176 (2005) 2717–2725.
[7] J.A. Kilner, C.K.M. Shaw, Solid State Ionics 154–155 (2002) 523–527.
[8] V.V. Kharton, A.P. Viskup, A.V. Kovalevsky, E.N. Naumovich, F.M.B. Marques, Solid State Ionics 143 (3–4) (2001) 337–353.
[9] G. Amow, I.J. Davidson, S.J. Skinner, Solid State Ionics 177 (13–14) (2006) 1205–1210.
[10] F. Mauvy, J.M. Bassat, E. Boehm, J.P. Manaud, P. Dordor, J.C. Grenier, Solid State Ionics 158 (1–2) (2003) 17–28.
[11] Q. Li, H. Zhao, L. Huo, L. Sun, X. Cheng, J.C. Grenier, Electrochem. Commun. 9 (2007) 1508–1512.
[12] J.M. Bassat, P. Odier, A. Villesuzanne, C. Marin, M. Pouchard, Solid State Ionics 167 (3–4) (2004) 341–347.
[13] C. Lalanne, F. Mauvy, J.M. Bassat, J.C. Grenier, P. Dordor, P. Stevens, in: M. Mogensen (Ed.), Proceedings of the Sixth European SOFC, 2004, p. 1351–1359, ISBN 3-905592-15-0.
[14] C. Lalanne, Thesis, 2005, Bordeaux 1 University.
[15] F. Mauvy, C. Lalanne, J.M. Bassat, J.C. Grenier, H. Zhao, P. Dordor, P. Stevens, J. Eur. Ceram. Soc. 25 (2005) 2669–2672.
[16] .A. Douy, Int. J. Inorg. Mater. 3 (2001) 699–707.
[17] J.N. Audinot, Thesis, 1999, Bordeaux 1 University.
[18] R.A. De Souza, J.A. Kilner, Solid State Ionics 106 (1998) 175–187.
[19] M. Molinelli, D. Larrain, R. Ihringer, L. Constantin, N. Autissier, O. Bucheli, D. Favrat, J. S Van herle, in: S. Singhal, M. Dokiya (Eds.), Proceedings of the Eigth International Symposium on SOFC Electrochemical Society, vols. 2003–2007, Paris, 2003, p. 905.
[20] L. Constantin, R. Ihringer, O. Bucheli, J. Van herle, in: J. Huijsmans (Ed.), Proceedings of the Fifth European SOFC, 2002, p. 132.
[21] R. Takeda, R. Kanno, M. Noda, Y. Tomida, O. Yamamoto, J. Electrochem. Soc. 134 (1987) p2656.
[22] Y.J. Leng, S.H. Chan, K.A. Khor, S.P. Jiang, Int. J. Hydrogen Energy 29 (2004) 1025–1033.
[23] J. Van herle, R. Ihringer, R. Vasquez Cavieres, L. Constantin, O. Bucheli, J. Eur. Ceram. Soc. 21 (2001) 1855–1859.
[24] C. Laberty, F. Zhao, K.E. Swider-Lyons, A.V. Virkar, Electrochem. Solid State Lett. 10 (10) (2007) B170–B174.
[25] C. Lalanne, F. Mauvy, J.M. Bassat, J.C. Grenier, P. Stevens, G. Prosperi, J. Van herle, S. Diethelm, R. Ihringer, in: M. Kilner (Ed.), Proceedings of the Seventh European SOFC, 2006, p. B0603-123.
[26] T. Tsai, S.A. Barnett, J. Electrochem. Soc. 142 (1995) 3084–3087.
[28] V. Dusastre, J.A. Kilner, Solid State Ionics 126 (1–2) (1999) 163–174.
[29] A. Ringuedé, J. Fouletier, Solid State Ionics 139 (3–4) (2001) 167–177.
[30] F. Mauvy, C. Lalanne, J.M. Bassat, J.C. Grenier, H. Zhao, L. Huo, P. Stevens, J. Electrochem. Soc. 153 (8) (2006) A1547–A1553.